Discussion of x-ray-absorption near-edge structure: Application to Cu in the high-T_c superconductors $La_{1.8}Sr_{0.2}CuO_4$ and $YBa_2Cu_3O_7$

Farrel W. Lytle and Robert B. Greegor
The Boeing Company, Seattle, Washington 98124

Armand J. Panson
Westinghouse Research and Development Center, Pittsburgh, Pennsylvania 15235
(Received 24 June 1987; revised manuscript received 26 August 1987)

A model for interpretation of x-ray-absorption near-edge structure (XANES) in transition-metal compounds is presented based on $\lambda = R$ backscattering from nearby atoms. The model allows identification of XANES features with specific lattice distances. Reference to spectra from model compounds of simple structure allows construction of a calibration curve of ΔE vs R from 1.5 to 3.5 Å with an accuracy of ± 0.1 Å. Specific multiscattering paths were also identified in MO_4 molecules. The Cu K spectra of $La_{1.8}Sr_{0.2}CuO_4$ and $YBa_2Cu_3O_7$ were examined using the model. A unique feature in the spectra was identified with a Cu—O bond distance of ~2.6 Å and confirmed with analysis of the extended x-ray-absorption fine structure. This distance is evidence of antisite disorder in these compounds with 0.2 ± 0.1 mole fraction of Cu substituting into the Y or La site. We also find evidence of simultaneous Cu^{2+} and Cu^{3+} valences. The structural implications of these findings are discussed.

INTRODUCTION

The shift in energy of the x-ray-absorption edge with change in valence has been used for many years to establish the valence in unknown materials.[1] Recently a number of studies have appeared of the Cu K absorption edge in the superconducting compounds $La_{2-x}Sr_xCuO_4$ and $YBa_2Cu_3O_7$ in order to establish the valence of Cu. The conflicting results claimed to find Cu^+ and Cu^{2+} in reduced La-Sr-Cu-O,[2] only Cu^{2+} in La-Sr-Cu-O,[3] Cu^{+2} and Cu^{+3} in La-Sr-Cu-O and La_2CuO_4,[4] and Cu^{+2} and Cu^{+3} in Y-Ba-Cu-O.[5] Since many of the differing explanations refer to identical spectra, there is an obvious lack of understanding as to the origin of the features on and near the x-ray-absorption edge, usually termed the x-ray-absorption near-edge structure (XANES). Herein we used an extensive set of reference spectra to demonstrate in detail for the first time the origin of the XANES spectra for K absorption in the transition metals. Identification of various XANES features with scattering from first- and higher-neighbor atoms allowed the construction of an empirical calibration curve of energy versus bond length, which allowed an accurate determination of bond distance(s) from the edge spectra. This calibration curve identified a prominent feature in the XANES of La-Sr-Cu-O and Y-Ba-Cu-O as a scattering resonance caused by a Cu bond distance of ~2.6 Å instead of a feature due to Cu^{3+}.[4] The ~2.6 Å distance was confirmed as a Cu—O bond in Y-Ba-Cu-O and La-Sr-Cu-O by analysis of the extended x-ray-absorption fine structure (EXAFS) and interpreted as evidence of antisite disorder, i.e., Cu substitution into the Y/La site. A discussion of antisite disorder in perovskites is given to place this result in context with the literature. Finally, we demonstrate that the presence of Cu^{2+} and Cu^{3+} can be confirmed in La-Sr-Cu-O and Y-Ba-Cu-O. Furthermore, separate crystallographic information was derived for the two different Cu valences.

EXPERIMENTAL DETAILS

Most of the spectra were obtained at Stanford Synchrotron Radiation Laboratory using a double crystal Si(220) monochromator with accurately set 1 mm slits which correspond to an angle of 5×10^{-5} rad. The exceptions were the Cu edges in Figs. 8 and 9. These spectra were obtained with the Si(440) reflection (1 mm slits) using two absorption lengths of aluminum to filter out the simultaneous lower energy (220) reflection. The intent was to obtain the maximum resolution possible, 0.4 eV (440) vs 1.2 eV (220) bandwidth at the Cu edge, in order to detail features in the smoothly varying absorption rise of La-Sr-Cu-O and Y-Ba-Cu-O. There was no significant difference in these spectra observed with the (440) reflection; however, the Cu, Cu_2O, and CuO spectra sharpened considerably. All of the solid, concentrated compounds were in the form of finely ground Duco smears and the spectra were obtained in the normal absorption mode. The solutions (approximately 1 M) and dilute solids were measured by the fluorescence technique. In all cases, reference metal spectra were obtained to establish a permanent energy calibration. All of the spectra are plotted in the figures with the zero of energy equal to the first inflection point of the respective metal.

The sintered oxides $La_{1.8}Sr_{0.2}CuO_4$ and $YBa_2Cu_3O_7$ were prepared from oxides and carbonates by mixing stoichiometric amounts and reacting in flowing oxygen for 16 h at 1000 and 940 °C, respectively. The reaction mixtures were reground, the same heat treatment repeated, and reground again.[6,7] X-ray diffraction powder patterns showed that the La-Sr-Cu-O was single-phase, K_2NiF_4

structure and the Y-Ba-Cu-O was the single-phase, orthorhombic, Perovskite-related phase.[8] The midpoints in the transition temperature curves were at 94 and 36.5 K for Y-Ba-Cu-O and La-Sr-Cu-O, respectively.[8] Panson[9] determined by classical wet chemical methods that the Y-Ba-Cu-O samples used here which were cooled slowly in O_2 contain Cu^{3+} in contrast to samples quenched from above 700 °C which do not. Two different reactions were used. Oxygen evolution measurements were done for samples dissolved in HCl where the reaction involves reduction of Cu^{3+} by water:

$$Cu^{3+} + \tfrac{1}{2} H_2O \rightarrow Cu^{2+} + H^+ + \tfrac{1}{4} O_2 \uparrow .$$

The oxygen was measured volumetrically. In a separate analysis acid dissolution in the presence of KI resulted in the reduction of Cu^{3+} by I^- to form I_2 which was then titrated by thiosulfate. The titration results showed 7.00 ± 0.02 oxygens per formula unit in Y-Ba-Cu-O; therefore, the formulas are $YBa_2(Cu_2^{2+}Cu_1^{3+})O_7$ and $La_{1.8}Sr_{0.2}(Cu_{0.8}^{2+}Cu_{0.2}^{3+})O_4$. Similar results using the same techniques were found by Manthiram *et al.*[10] For $YBa_2Cu_3O_7$ thermogravimetry also provided the oxygen composition which agreed with the titration results.[8] These simple, chemical measurements are a sure determination of the $[Cu^{2+}]/[Cu^{3+}]$ composition of the materials. The edge data confirm these valence assignments in a general way, but are much more sensitive to the nearby coordination environment.

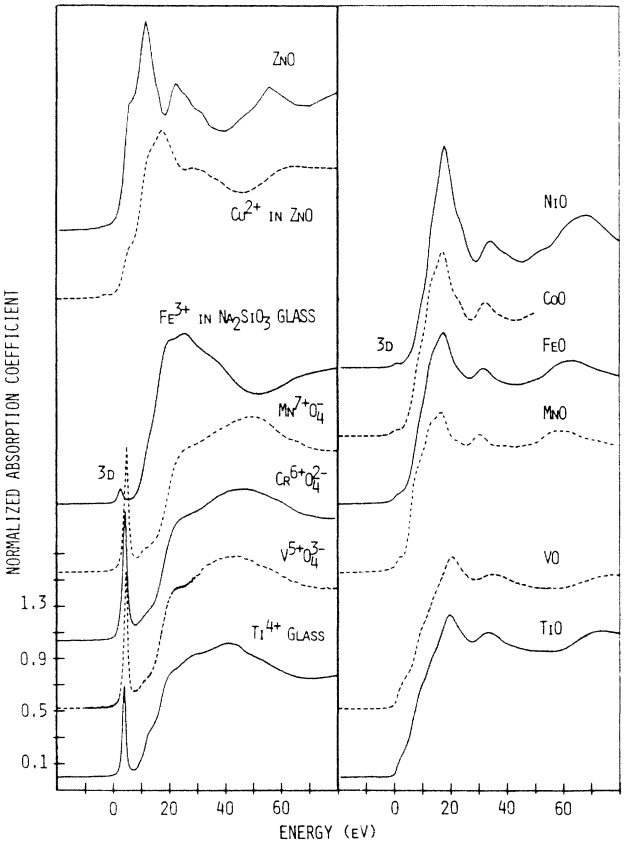

FIG. 1. XANES of transition metals in tetrahedral (left) and octahedral (right) coordination. The zero of energy corresponds to the first inflection point of the corresponding pure metal in Figs. 1 and 4–8.

EXPLANATION OF XANES

In the work of Sette, Stöhr, and Hitchcock[11] and Stöhr, Sette, and Johnson[12] the spectra from simple molecules in the gas phase[11] and chemisorbed on Pt (Ref. 12) were used to derive a simple relationship between bond distance and the energy position of a feature termed the σ^* resonance. The σ^* resonance was obvious in their data because it was broader than the immediately preceding bound-state transitions and was identified in a general way with scattering from the adjacent atom(s). Bianconi, Fritsch, Calas, and Petiau[13] made a similar connection of the first broad peak with the first short bond in the series of $3d^\circ$ compounds, Ti^{4+}, V^{5+}, and Cr^{6+}, all coordinated by O_4. We present a similar, but more extensive set of data in Fig. 1 where we plot data for compounds of most $3d$ elements in tetrahedral and octahedral coordination. Where possible, we use data for the tetrahedral ions in solution, in H_2O or in glass, reasoning that the lack of long-range order will minimize the occurrence of scattering from second and higher neighbors[13] which could confuse our interpretation. The 3 wt.% TiO_2 in SiO_2 has been shown to be in tetrahedral oxygen coordination.[14] The Fe^{3+} in Na_2SiO_3 glass was shown by Mössbauer measurements to be in tetrahedral oxygen coordination.[15] The 1 wt.% CuO in ZnO was shown by EXAFS to be in fourfold coordination.[16]

For examples of octahedral coordination we used the NaCl-type MO compounds, which were available for most of the $3d$ elements. We expect pure octahedral spectra, although in some of the compounds there are vacancies in either or both of the metal and oxygen sites, particularly TiO, VO, and FeO.[17] All of the spectra of compounds with a $3d$ vacancy show a pre-edge feature which is a $1s$ to $3d$ transition. This varies in intensity with the number of d vacancies and with the symmetry of the absorbing atom site. For tetrahedral atoms it is dipole allowed and prominent. For an atom with inversion symmetry, it is (primarily) the much weaker quadrupole transition. This has been experimentally demonstrated by Hahn *et al.*[18] The theoretical[19] and experimental variation of this $1s$ to $3d$ peak in a series of compounds has been demonstrated for Ti (Refs. 14 and 20), V (Ref. 21), and Cu (Ref. 22). This transition is so weak in Cu compounds as to be of little use as a diagnostic, although the absence of a transition confirms Cu^+. The paper of Kau *et al.*[22] examined a very large series of primarily metal-organic Cu^+ and Cu^{2+} compounds and classified the spectra according to structure type. It was demonstrated that mixtures of Cu^+ and Cu^{2+} could be unambiguously identified. This paper also identified the sharp peak halfway up the edge in Cu_2O and CuO (Fig. 8) as the $1s$ to $4p$ transition. This is an important identification. Since we expect no significant or narrowly defined bound-state transitions at higher energies, we interpret all of the absorption rise beyond this $4p$ transition as due to some other effect.

All of the short-bond MO_4 spectra are very similar

showing a trend of the first broad maxima to higher energy as R decreases.[13] All of the cubic MO compounds are similar to each other, showing a sharp absorption rise to a large, narrow peak followed by a smaller, relatively sharp second peak. Assuming that KR = const.,[23] or ER^2 = const.,[13] the following peak assignments can be made. (Note that the two expressions for R are equivalent.) If the broad peak at 40–50 eV in the MO_4 ions is due to single scattering from the four first-neighbor oxygen atoms at 1.6 Å, then the second peak in the MO spectra at ~30 eV is due to single scattering (SS) from the six first-neighbor oxygen atoms at about 2 Å and the peak at the top of the edge at ~15 eV is due to SS from the 12 second-neighbor metal atoms at about 3 Å. This follows simply by letting the free-electron wavelength $\lambda = h/mv = R$ with the expectation that simple backscattering will be more intense than any multiple scattering. Neglect of any phase shift should produce errors small enough so that XANES peaks can be assigned to specific coordination shells. This identification of peaks in the absorption edge with particular lattice sites allows construction of a calibration curve in the same spirit as Sette *et al.*,[11] Stöhr *et al.*,[12] and Bianconi *et al.*,[13] except that here the range of correlation can be extended to the full region of $\lambda = R_n$, i.e., from 1.5–3.5 Å including second neighbors in this data. The bond distances and measured energies of the absorption maxima are given in Table I and plotted in Fig. 2 along with the condition for the free-electron wavelength $\lambda = R_n$. Also included is data for fcc Cu, Ni, and Co to be discussed later. Following Bianconi *et al.*[13] ΔE is defined as the interval between the $1s$ to $3d$ prepeak and the feature of interest. We submit that this correlation is remarkable and confirms the peak assignments, particularly in view of the simple structures of the reference compounds. This calibration may be converted into a ruler[12] which can be used to overlay edge spectra and read the bond distances of the first two neighbors to an accuracy better than ±0.1 Å. Examples are shown later. The correlation should be linear with $1/R^2$ and is plotted in Fig. 3, along with the equivalent $\lambda = R_n$ condition, $E = 150/R^2$. There are some additional data

TABLE I. Bond distances (Ref. 17) and XANES peak assignments.

Sample	R_1 (Å)	ΔE (eV)	R_2 (Å)	ΔE (eV)
$Ti^{4+}O_4/SiO_2$	1.79	37.1		
$V^{5+}O_4/H_2O$	1.74	38.7		
$Cr^{6+}O_4/H_2O$	1.68	41.5		
$Mn^{7+}O_4/H_2O$	1.63	44.3		
TiO	2.09	32.4	2.95	18.5
VO	2.05	34.4	2.89	19.0
MnO	2.22	28.2	3.14	14.3
FeO	2.16	29.7	3.05	15.1
CoO	2.13	31.9	3.02	16.4
NiO	2.08	33.0	2.95	16.6
Cu	2.56	21.6		
Ni	2.49	22.8		
Co	2.51	22.0		

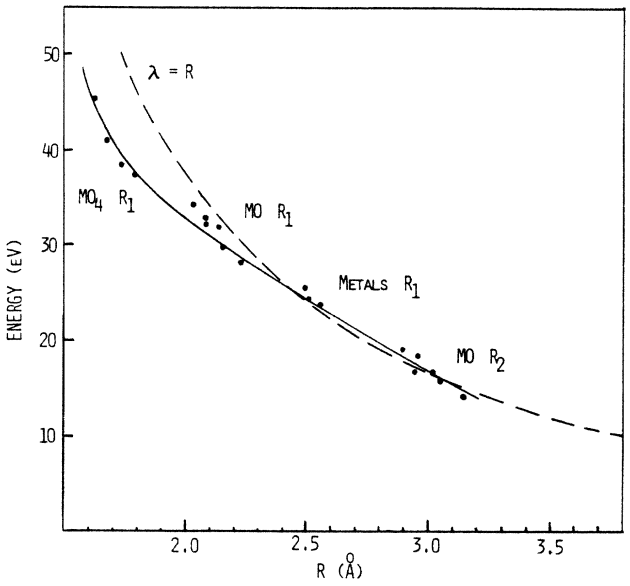

FIG. 2. A plot of the data in Table I, ΔE vs R_n. The various groups of data points are identified for the first neighbors R_1 and second neighbors R_2 in the appropriate compounds. The condition that the free-electron wavelength, $\lambda = h/mv = R$, is shown by the broken line.

from the fcc metals Cu, Ni, and Co, where the zero of energy was chosen to be the first inflection point. Again identifying the second peak above the edge with SS from the nearest neighbors there is consistency with the data from the oxide compounds as shown by the plots in Figs. 2 and 3. Furthermore, the $1/R^2$ extended scale tempted us to see how far scattering from near neighbors was folded

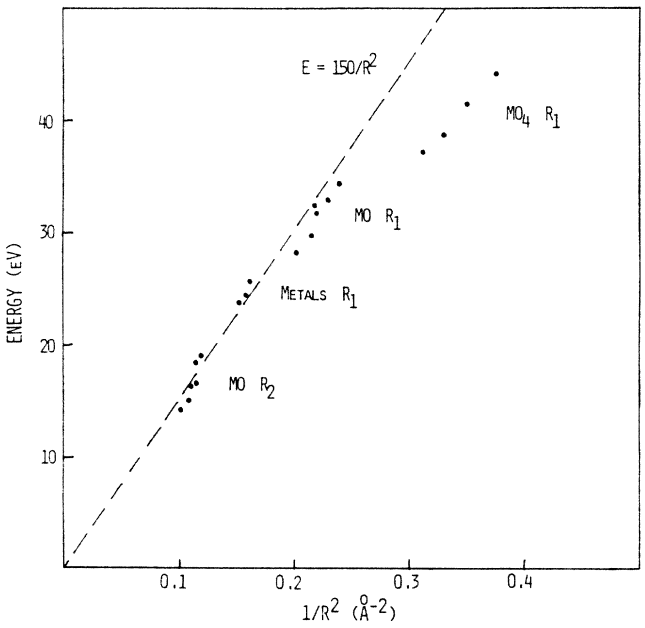

FIG. 3. A plot of ΔE vs $1/R_n^2$ for the data in Table I with the same notation as in Fig. 2.

back down the absorption edge and could be identified with absorption features. In order to make the features in the edge more visible and to locate them more accurately in energy, we used a 5 eV straight-line running average (boxcar smoothing) on the data and then subtracted it from the original data file. The results for NiO and Cu metal are shown in Fig. 4 by the broken lines. The procedure did pull the peaks out of the smoother curves so that they were visible. Peaks, which were skewed by a sloping background, were corrected to nearer their true energy value; however, the amplitudes were not linearly related to the original peak amplitude, sharp features were emphasized. Nevertheless, they served as a useful guide to the eye. It was observed that in NiO features corresponding to good agreement with R through R_4 were visible. (We believe the high-energy shoulders at +8 eV from the R_1 and R_2 peaks to be multiple ionization images of the primary resonance. Similar features are seen in much of the data and appear to correlate with the expected ionization potential.) The agreement for Cu is not quite as good. The close packing collapses the structure so that the separate peaks are not clearly resolved. The subtraction procedure also makes visible a small feature at +4 eV from the $3d$ peak in NiO. We tentatively identify this with the $1s$ to $4p$ transition. It is similarly visible in many of the octahedral compounds. The step in the Cu metal edge has been identified traditionally with transitions to the peak in the band structure (d-bands) which occurs just above the Fermi energy E_f.

The effect of the phase shift is apparent as deviations from the case of the free-electron $\lambda = R$ approximation as shown by the dashed lines in Figs. 2 and 3. It is most significant for the short bonds in the high-valence MO_4 series. It is apparent that each subset of data has its own slope and calibration curve which happen to fall fairly near the $\lambda = R$ curve in this case. Data for other elements could be expected to not be exactly the same as these but would construct their own calibration curve depending upon the magnitude(s) of R_n and the location of $E = 0$.

The importance of multiple scattering (MS) in XANES has been addressed recently by a number of papers. From calculations Norman *et al.*[24] concluded that in NiO MS was important up to 30 eV from the edge; however, Muller and Schaich[25] demonstrated that an SS calculation for Cu metal was adequate if the spherical wave nature of the photoelectron was included. Stöhr *et al.*[26] identified MS features in molecules with short bonds. Bunker and Stern[27] reported an interesting experiment which showed that two features in XANES of solid $KMnO_4$ were temperature sensitive. They also emphasized the point originally made by Boland, Crane, and Baldeschweiler[28] that when the angle between the first and last scattering path is equal to 90°, MS cancels out, e.g., in octahedral symmetry. MS in these compounds can occur for the case of the more distant atoms which are in direct line with the nearest neighbor atoms. Our choice of

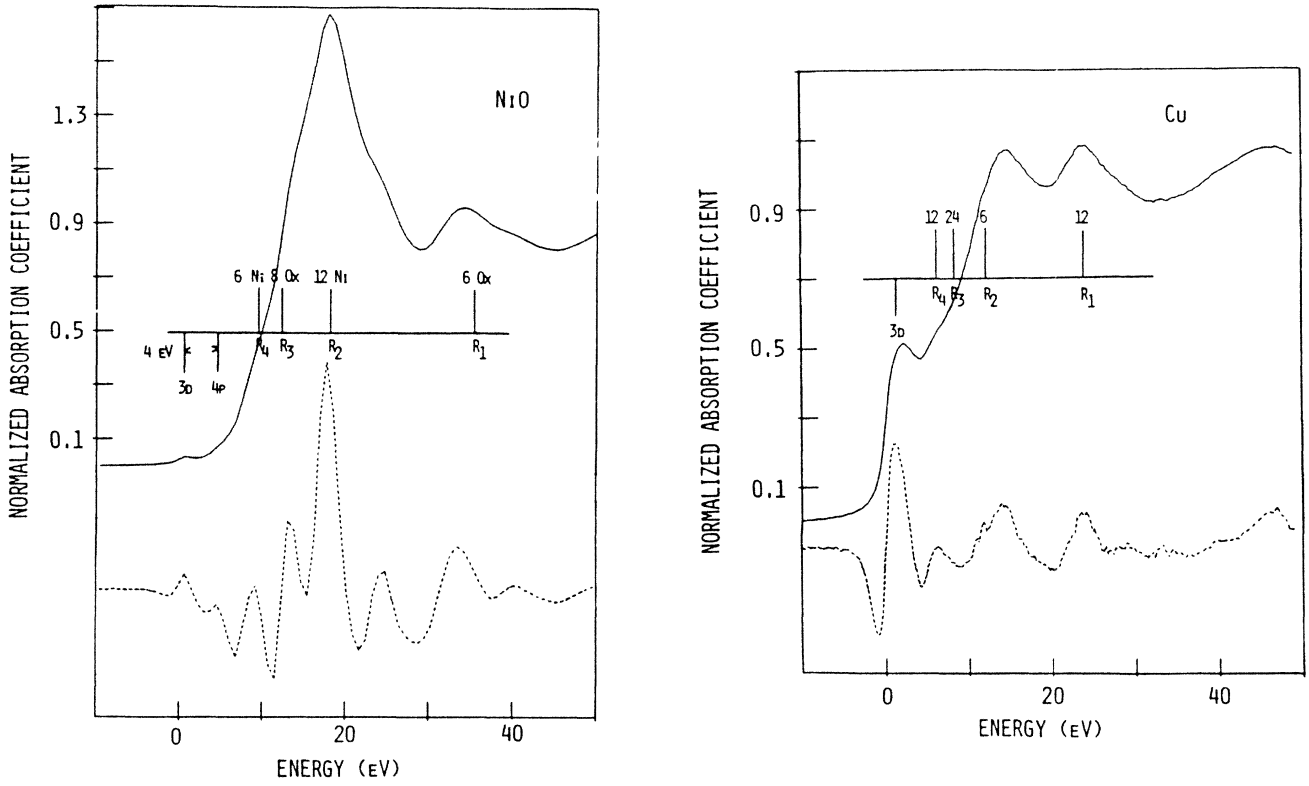

FIG. 4. XANES spectra for NiO and Cu metal. The dashed line at the bottom is the result of subtracting a 5 eV running average from the original data set in order to make the features in the steeply rising edge more visible. The agreement with known lattice distances is shown by the R_n distances along the labeled horizontal line.

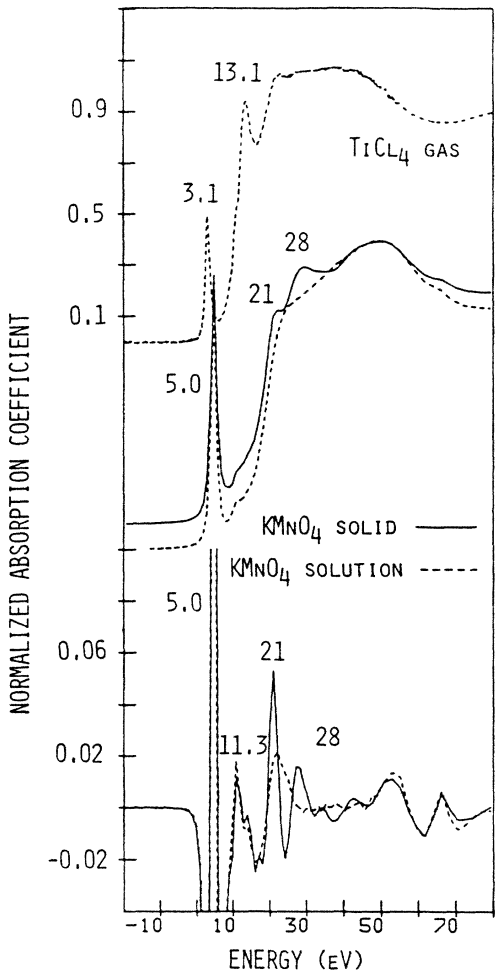

FIG. 5. Identification of SS and MS features in tetrahedral molecules. The various features are identified in the text. The broad absorption maximum in $TiCl_4$ gas is unnaturally compressed because the sample was too thick.

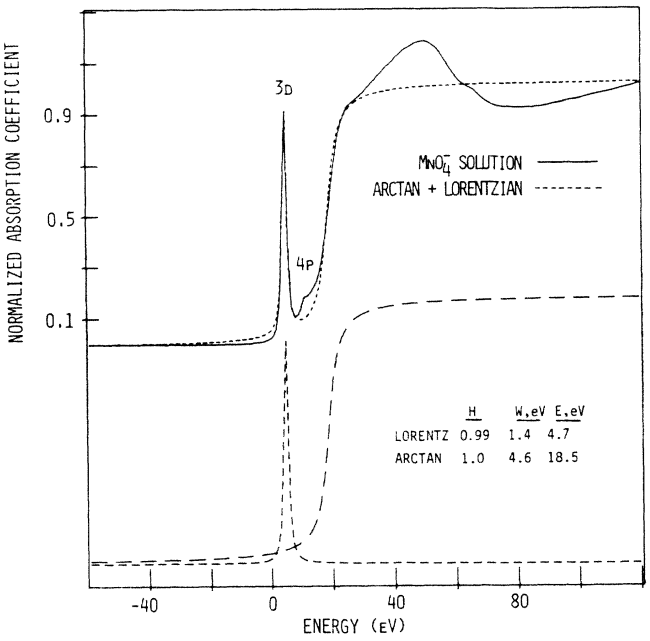

FIG. 6. In the top portion the sum of an arctangent and a Lorentzian are fitted to the MnO_4^- solution data. The individual components and fitted parameters are given below.

octahedral MO compounds in Fig. 1 was because of this factor. On the other hand in molecules without inversion symmetry such as tetrahedral MO_4, MS can occur. Since scattering is proportional to $1/R^n$ the largest effect will be for the shortest possible MS distances, i.e., within the first coordination shell. The two possible MS paths are $M-O-O-M$ and $M-O-M-O-M$ which are equal (divided by 2) to $1.816R_1$ and $2R_1$, respectively. With spectra chosen from selected samples it was possible to unambiguously identify the MS features in Fig. 5. At the top is the Ti K edge of gas-phase $TiCl_4$. In an isolated molecule only SS from the 4 Cl and MS around the tetrahedron are possible. The broad SS peak has already been identified as due to the Ti-Cl bond of 2.185 Å and the peak at 13.1 eV must be due to the MS path Ti—Ci—Cl—Ti, which should be strongest. In the middle of Fig. 5 data from solid $KMnO_4$ and a 1 M aqueous solution (both at 25 °C) are overplotted. MS around the tetrahedron should occur in both, but SS (or MS) from more distant neighbors can occur only in the solid. In order to make the structure more visible, the 5 eV running average was applied and plotted at the bottom of Fig. 5. Note that this treatment emphasized the sharp peaks. Since the 28 eV peak was totally missing from the solution spectrum, it was identified as SS from more distant atoms at ~2.6 Å. The peak at 21 eV is present in both solution and solid and must be due to the MS path Mn—O—O—Mn. The 21 eV peak is broadened in solution, perhaps by thermal disorder. Both the 21 and 28 eV peaks were found to be temperature sensitive in the solid.[27] The ΔE values, R_n from Fig. 2 and $R_{MS}=1.816R_1$ are listed in Table II with good agreement between the known value of R_{MS} and R_{MS} (graph). The apparent visibility of this MS feature is sensitive to its position on top of the continuum rise and becomes more visible when R_{MS} is long enough to move it down the edge as

TABLE II. Identification of multiple-scattering peaks.

Sample	3d (eV)	4p (eV)	$\Delta E=E-E_{3d}$	R_{MS} from graph (Å)	$R_{MS}=1.816R_1$ (Å)
$TiCl_4$	3.1	10.7	10.0	3.8	3.97
$KMnO_4$	5.0	11.3	16	3.0	2.96
MnO_4/H_2O	5.0	11.3	17	3.0	2.96

in $TiCl_4$. The $1/R^2$ compression of the energy scale also narrows the peaks as they move closer to $\Delta E = 0$. Note that the MO_4^- solution data in Fig. 1 all show this feature once one knows what to look for. Bianconi *et al.*[13] noted that the MS peak and the SS from R_1 both scaled as $1/R^2$, but apparently considered both to be due to MS and did not specifically identify either scattering path. The energies of the $3d$ and $4p$ transitions relative to the first inflection point of the metal are also given in Table I. The $4p$ transition is identified by default. It is expected to be present and there are no other features at higher energy. In MnO_4^- solution spectra, as in Fig. 5 where there is no long-range order, the sharp rise at the absorption edge is featureless and one can see the pure continuum arctangent curve ascending underneath. This is demonstrated in Fig. 6 where we have fitted a Lorentzian and arctangent to the MnO_4^- data. The individual functions are given along with their parameters—height, width, and energy position. Convolved with the fit was the Gaussian resolution function of 0.6 eV width.

The reason these low-energy scattering maxima are strong relative to the higher energy EXAFS is because of the high scattering cross section for low-energy electrons, just the inverse of the "universal curve" of electron range versus energy.[29] It also follows that trends in scattering by different atom types, i.e., different atomic numbers Z and different numbers of scatterers, will be evident in the XANES. This is shown by the series of MO compounds in Fig. 1. The intensity of the peak from the 6 O first neighbors at -30 eV remains about the same throughout the series; however, the 12 second-neighbor metal peak at -15 eV increases in a linear way as Z increases from Ti to Ni. Previous assignments of this peak as a $1s$ to $4p$ transition are wrong. There is a $1s$ to $4p$ transition at lower energy as we have shown. In Cu compounds[22] it becomes visible in nonoctahedral coordination at 6.8 eV in CuO or 3.0 eV in Cu_2O (Fig. 8).

The Jahn-Teller splitting of Cu $3d^9$ provides a wonderful variation in structure and hence in the K spectra. Figure 7 displays spectra from variously distorted octahedral Cu environments on the left and a progression to perfectly square planar on the right. Also included is the calibrated ruler from Fig. 2 along the top. These spectra provide an impression of the distance resolution possible with XANES. Unlike the sharply peaked first-neighbor interference at -30 eV which was present in all the MO compounds, here the peak is broadened, smeared, and even a doublet because the local environment is distorted. However, in CuO this peak from the 4 square planar oxygens is regular and the apical oxygens create a shoulder at 20 eV. The broad, first-neighbor peak in the square planar compounds at 30–40 eV is similar to the MO_4 spectra because there are only four scatterers rather than six. The peak is even sharper in Cu metal with 12 neighbors at 2.56 Å (Fig. 8). The broadened first peak above the edge in Fig. 7 also reflects the distorted environment of the

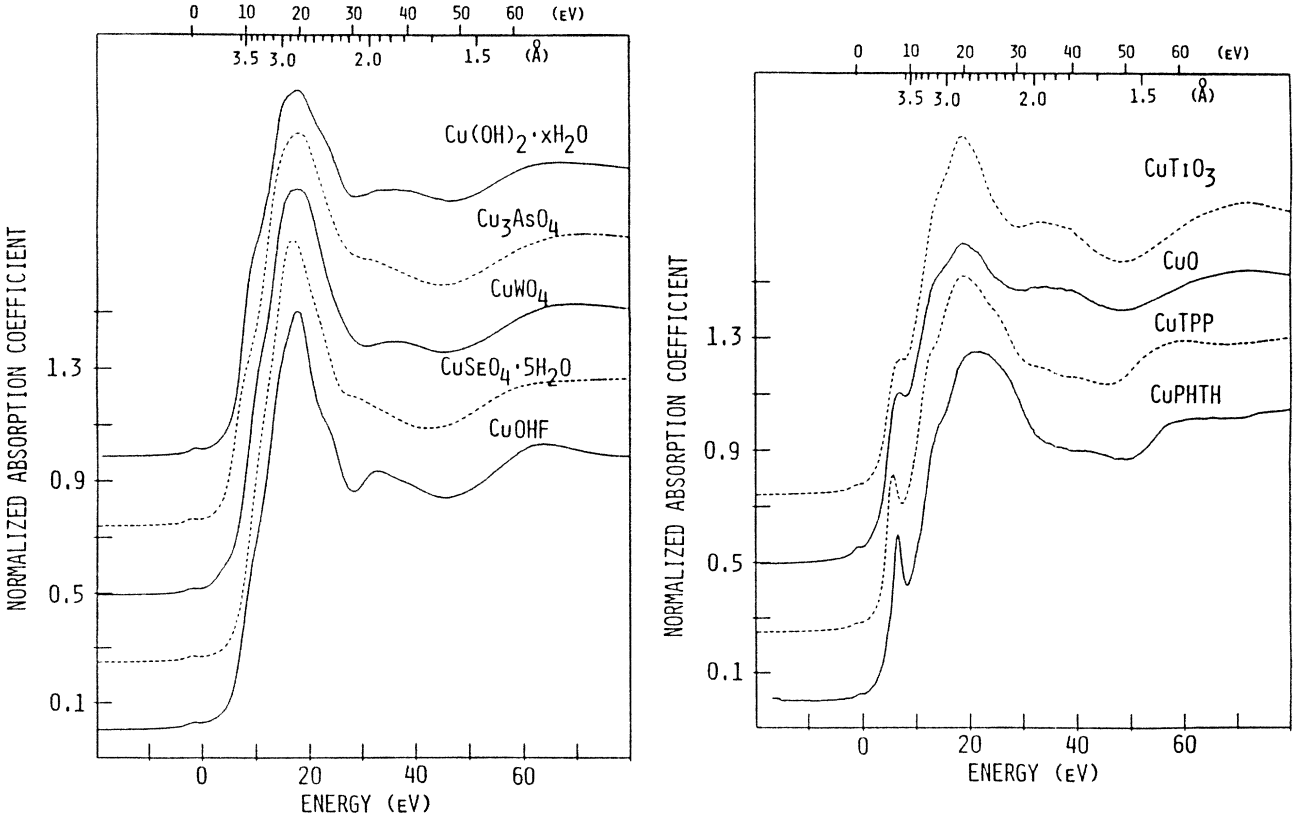

FIG. 7. Cu^{2+} in distorted octahedral coordination (left) and a progression from distorted octahedral coordination ($CuTiO_3$) to square planar coordination (Cu phthalocyanine) on the right. The (Å) scale at the top was derived from Fig. 2.

second neighbors, as well as the varying scattering amplitudes from different kinds of atoms. The sharpness of the 1*s*-to-4*p* transition is shown to be a sensitive function of the symmetry change from distorted octahedral in $CuTiO_3$ to perfectly square planar in Cu phthalocyanine.

APPLICATION TO La-Sr-Cu-O AND Y-Ba-Cu-O

We now apply the above observations to XANES spectra of La-Sr-Cu-O and Y-Ba-Cu-O. The shift in energy with valence is shown in Fig. 8 for Cu, Cu_2O, CuO, and La-Sr-Cu-O. The shift occurs near the bottom of the absorption edge and all the spectra overlap near the top. It would be easy to conclude that La-Sr-Cu-O and Y-Ba-Cu-O, which have very similar spectra, contain a significant fraction of Cu^{3+}; however, the edge position is determined not by valence alone, but also by bond distance and the way the scattering from neighboring atoms folds back down the edge. The spectra of *all* the distorted octahedral compounds on the left in Fig. 7 show an even greater shift at the bottom of the edge than La-Sr-Cu-O and Y-Ba-Cu-O and they are all pure Cu^{2+}. A paper by Hu, Chan, and Brown,[30] which showed no spectra, mentioned that edge features in four Cu^{3+} compounds were similar in energy to Cu^{2} compounds. Similar considera-

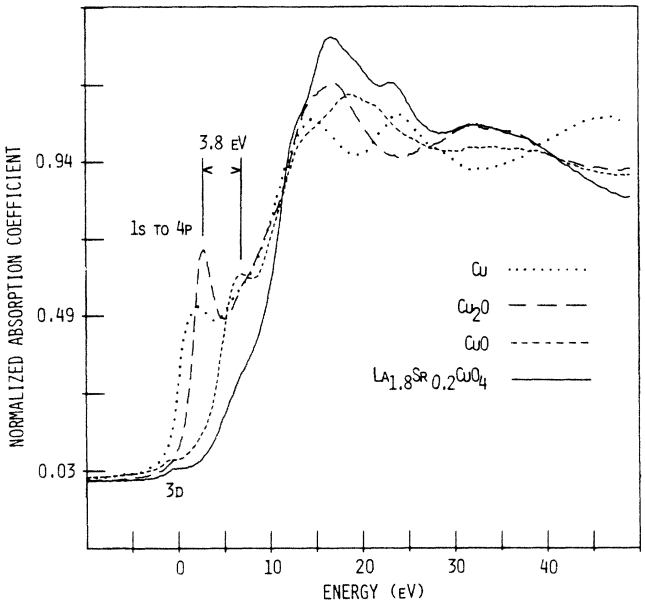

FIG. 8. The chemical shift of the absorption edge with increasing valence for Cu, Cu_2O, and CuO. The edge of La-Sr-Cu-O is also shown for comparison; Y-Ba-Cu-O is nearly identical. Note the 3.8 eV shift of the 1*s* to 4*p* transition from Cu_2O to CuO.

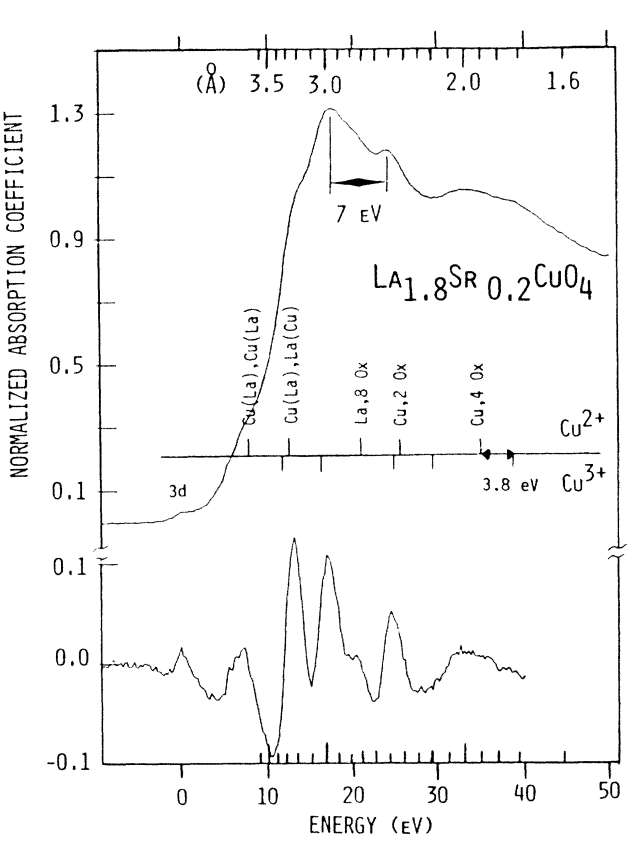

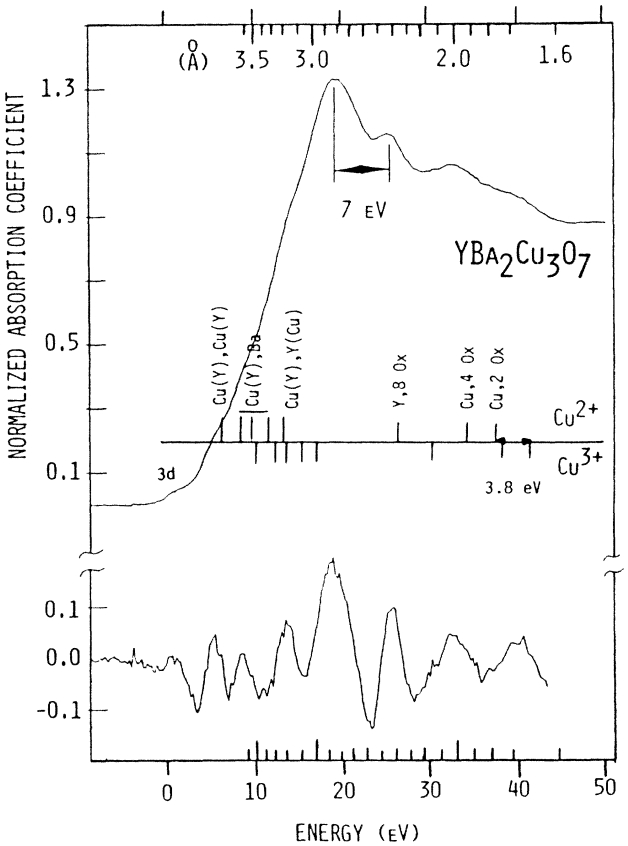

FIG. 9. Absorption coefficient vs energy (eV) and radial distance (Å) for $La_{1.8}Sr_{0.2}CuO_4$ and $YBa_2Cu_3O_7$. The zero of energy is the 3*d* peak, the Å scale is from Fig. 2. The labeled, horizontal line indicates possible bond distances from Table III with Cu^{2+} and Cu^{3+} below (shifted by 3.8 eV). The graph at the bottom is the result of subtracting a slightly smoothed curve from the original data set as in Fig. 4. The feature at +7 eV from the absorption maximum was deduced to be due to Cu occupying the Y and La sites.

tions led Tranquada, Heald, Moodenbaugh, and Suenaga[3] to conclude that only Cu^{2+} is present in La-Sr-Cu-O particularly since the spectrum of La_2CuO_4 (formally Cu^{2+}) was identical with La-Sr-Cu-O. Alp *et al.*[4] also measured the spectra of $KCuO_2$ (valence 3^+) and found an absorption rise similar to La-Sr-Cu-O and shifted 2 eV to higher energy. They identified the 7 eV doublet (Fig. 9) at the top of the edge as the Cu^{2+}, Cu^{3+} components and assigned a mix of Cu^{2+} and Cu^{3+} valences to La-Sr-Cu-O *and* La_2CuO_4, which is chemically inconsistent. As noted below we believe 7 eV to be too large a shift. Oyanagi *et al.*[2] measured a preparation of La-Sr-Cu-O which had a strong component from Cu^+ similar to Cu_2O and claimed that Cu^+ and Cu^{2+} were in the sample. Oyanagi *et al.*[5] also examined Y-Ba-Cu-O, compared it to CuO, and claimed it was predominately Cu^{2+} with a small Cu^{3+} component, but without explaining their reasoning in detail. We attempted to test the sensitivity of the Cu *K* edges to the mix of $[Cu^{2+}]/[Cu^{3+}]$ simply by adding the edge to itself after shifting for Cu^{3+} and scaling to the expected $[Cu^{2+}]/[Cu^{3+}]$ ratio. In general we found the results indistinguishable from the original. These edges have so many features and are so broad that they are quite insensitive. However, in work in progress, we have measured the Cu $L_{2,3}$ spectra where the $2p$ to $3d$ transitions are dipole allowed and become edge resonances. Here we find the resonance intensity in La-Sr-Cu-O and Y-Ba-Cu-O to increase as expected for the Cu^{2+} and Cu^{3+} components.[31]

Our data for La-Sr-Cu-O and Y-Ba-Cu-O are given in Fig. 9. The spectra are similar to each other and apparently identical to the spectra for the same compounds measured by the other investigators already discussed. Hence, we are all interpreting the same spectra with the exception of the Cu^+ containing La-Sr-Cu-O examined by Oyanagi *et al.*[2] Recognizing the different physical processes which makeup the absorption rise and noting the 3.8 eV shift from Cu^+ to Cu^{+2} of the $1s$ to $4p$ transition, we conclude that the doublet at the top of the edge spread by 7 eV is not a reasonable result for mixing Cu^{2+} and Cu^{3+} as was suggested by the interpretation and peak assignments of Alp *et al.*[4] We believe that the Cu^{2+} and Cu^{3+} edge shift should be about the same as the $1s$ to $4p$ shift from Cu^+ to Cu^{2+}, i.e., 3.8 eV. We assume this value and apply it to shift the distance scales for edge features identified with Cu^{3+}. It is not a critical assumption for our major conclusions. For comparison, data for V compounds had a shift of 1–2 eV per valence unit as valence varied from V^{3+} to V^{5+}.[21] In order to make the true structure in the edge more visible we applied the 5 eV running average and subtraction technique to the La-Sr-Cu-O and Y-Ba-Cu-O data with the results shown at the bottom of the plots in Fig. 9. In each spectrum many different bond distance peaks were resolved. This is the result of the complex crystal structure and the 2 Cu valences with Cu^{3+} shifted +3.8 eV relative to Cu^{2+}. The labeled line across the center indicates the crystallographically expected distances in the neighborhood of the Cu atoms with possible Cu^{2+} distances above the line and possible Cu^{3+} distances below. The structure determination of La-Sr-Cu-O by Cava, Santoro, Johnson, and Rhodes[32] and of Y-Ba-Cu-O by LePage *et al.*[33] were used and are listed in Table III. The energy locations corresponding to the crystallographic distances were determined from the calibration curve of Fig. 2. There is fair agreement with most of the peaks except for the prominent peak corresponding to approximately 2.6 Å. This feature at +7 eV from the absorption maximum is the distinguishing feature of these edges and also that of La_2CuO_4.[3,4] In order to account for this distance we must assume that Cu is substituting into the Y (Y-Ba-Cu-O) and La (La-Sr-Cu-O and La_2CuO_4) sites. Thus, our interpretation is that the distinguishing feature of these edges which has been attributed to Cu^{3+} (Ref. 4) is actually due to a scattering resonance from a bond distance of ~2.6 Å. It follows that the presence of Cu^{3+} is not necessary to explain the XANES of La_2CuO_4. Furthermore, the relative peak intensities in the XANES in Fig. 9 suggest the Cu is present in both valences in the Y or La sites with $[Cu^{2+}] > [Cu^{3+}]$ in Y-Ba-Cu-O and $[Cu^{3+}] > [Cu^{2+}]$ in La-Sr-Cu-O. In the normal Cu sites Cu^{2+} appears to predominate. The general appearance of the edge is due to the staggered distribution of neighbors which spreads out the edge and introduces many small features. In this instance the chemical analyses were a more certain indication of valence than was the absorption

TABLE III. Atomic environment in $YBa_2Cu_3O_7$ (Ref. 33) and $La_{1.85}Sr_{0.15}CuO_4$ (Ref. 32).

$YBa_2Cu_3O_7$[a]			
Cu(1) site	Cu(2) site	Y site	Ba site
1.81, 2 O			
1.93, 4 O[b]	1.95, 4 O		
	2.35, 1 O	2.39, 8 O	
			2.75, 4 O
			2.91, 4 O
			2.98, 4 O
	3.20, Y	3.20, Cu(2)	
	3.36, Ba		3.36, Cu(2)
3.50, Ba			3.50, Cu(1)
		3.66, Ba	3.66, Y
3.85, Cu(1)	3.85, Cu(2)	3.85, Y	3.85, Ba
4.17, Cu(2)	4.17, Cu(1)		4.38, Ba

$La_{185}Sr_{0.15}CuO_4$[a]	
Cu site	La site
1.89, 4 O	
2.41, 2 O	2.35, 1 O
	2.64, 4 O
	2.73, 4 O
3.25, La	3.25, Cu
3.78, Cu	3.78, La
	3.96, La
4.77, La	4.77, Cu
5.32, Cu	5.32, La

[a]Oxygen atoms are listed only for the first coordination sphere.
[b]David *et al.* find only two oxygens at this distance [Nature **327**, 310 (1987)].

edge position. The identification of Cu^{3+} did not come from the absorption edge position but from chemical analyses. However, inclusion of Cu^{3+} and its edge shift of 3.8 eV resulted in a reasonable accounting of the XANES features shown in Fig. 9. The specification of Cu^{2+} or Cu^{3+} in the various sites is somewhat ambiguous and might be improved by simulation and fitting to the data.

ANALYSIS OF EXAFS

The theory and applications of EXAFS are now well known and have been widely applied.[34] However, it is not generally appreciated how sensitive EXAFS is to thermal disorder;[35] moreover, that the effect is dependent upon the correlated motion of the atoms comprising a specific bond. In anisotropic solids such as these there can be large thermal disorder for one bond and not for another. We examined the 25 °C EXAFS of La-Sr-Cu-O and Y-Ba-Cu-O and confirmed that the distances of ~2.6 Å were evident in the Fourier transforms as well as those expected from the normal Cu sites. This is shown in Fig. 10 and compared to CuO of known and more simple structure to get an appreciation of the resolution possible with an EXAFS transform. The 4+2 coordination of CuO is barely resolved at 25 °C because of the difference in thermal disorder between the two types of bonds. The lattice is stiff in the plane with most of the motion perpendicular to it in the direction of the apical oxygens.[36] The large thermal disorder of the apical bond causes the EXAFS to damp out in a couple of cycles, so that the peak in the transform is small. This distance is most evident in the first EXAFS bump where it appears as a shoulder on the first large peak at ~20 eV as shown in Figs. 7 and 8. At low temperatures the transform of this distance is much sharper with increased intensity.[37] The transforms of the 25° C EXAFS data for La-Sr-Cu-O and Y-Ba-Cu-O in Fig. 10 also resolve the Cu–O square planar bonds and the apical bonds plus the ~2.6 Å Cu–O bonds associated with Cu in the Y or La site. These are labeled in Fig. 10. Since the transforms were taken over a finite range $K = 2-14$, there are also small termination ripples which appear unavoidably on the sides of the main peaks and mix with the true structure peaks; however, the ripples move as the K range is changed whereas the structure peaks do not. Thus, these effects may be sorted out. For reasons similar to that discussed for CuO the apical and Y or La site Cu–O bonds have a large thermal disorder compared to the square planar bonds and the EXAFS damps out quickly. The largest effect due to the bond is present in the first EXAFS cycle (XANES) as has been discussed. In work in progress[37] we have examined data from Y-Ba-Cu-O at 77 K and found a large increase in intensity in the Fourier transform peaks due to the apical and Y site bonds consistent with the above discussion. Although it is not shown, we examined the imaginary part of the Fourier transform to confirm that it peaked with the magnitude for all these Cu–O bonds.

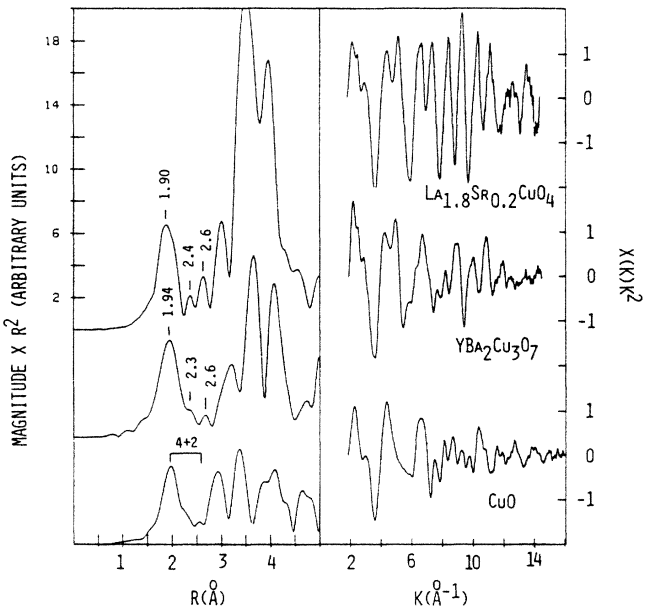

FIG. 10. The EXAFS (right) and Fourier transforms (left) of CuO, Y-Ba-Cu-O, and La-Sr-Cu-O are shown. The K^2, $K = 2-14$, Cu–O phase-corrected transforms were multiplied by R^2 in order to make the peak intensity approximately proportional to coordination number (for the same bond type). The 4+2 coordination of CuO is just resolved. The similar bonds plus those due to Cu in the Y or La site at ~2.6 Å are resolved in La-Sr-Cu-O and Y-Ba-Cu-O. All are plotted to the same scale.

All these different distances are evident in the work of others[3,38] but their significance was not realized. An important consideration when one is interested in more than the first bond distance is to multiply the transforms by R^2 to place the intensity of the Fourier transform peaks in more correct perspective relative to coordination number as was done in Fig. 10. These distances are beautifully resolved by Tranquada *et al.*[3] in the 10 K data for La-Sr-Cu-O and La_2CuO_4. Boyce *et al.*[38] analyzed variable temperature data on La-Sr-Cu-O (and $La_{1.8}Ba_{0.2}CuO_4$) to estimate that for the square planar bond, $\Theta_E = 610$ K and $\Theta_E = 500$ K for the apical bond. The bond due to Cu in the La site is evident in their data but was not recognized.[38] The distribution of Cu among the normal and Y or La sites was estimated from the relative transform peak amplitudes as measured from Fig. 10. The calculation accounted for the different coordination number of each site and the $1/R^2$ variation with peak amplitude. The EXAFS was also fitted in K space with a multishell fitting program. Both estimates gave a range of $x = 0.2 \pm 0.1$, thus the compounds would be written $(M_{2-x}Cu_x)(Cu_{1-x}M_x)O_4$ and $(Y_{1-x}Cu_x)Ba_2(Cu_{3-x}Y_x)O_7$. For charge balance we assume here that the M or Y atom displaced from its normal site must now occupy a Cu site. EXAFS from the Y or La edges should prove this. Unfortunately, we did not measure this spectra but others have.[3] We have made a graphical analysis of La L_1 data from Tanquada, Heald, and Moodenbaugh[39] and the O K-edge data of Yarmoff *et al.*[40] which confirms these assignments.[41]

DISORDER IN PEROVSKITE OXIDES ABO_3: LIMITATIONS OF STRUCTURE TECHNIQUES

The basic structure of perovskite-type crystals is composed of a close packing of oxygen atoms where every fourth one is replaced by an A atom. The B atoms are located in $\frac{1}{3}$ of the available octahedral interstices and their bonds to oxygen hold the crystal together. There is extensive solubility among various perovskites so that compounds of the form $(A_1,A_2)(B_1,B_2)O_3$ are common. There is also a region of tolerance to accommodate various sizes of atoms into the basic structure such that for the A site radii, $R_A = 1.2$–1.6 Å and for the B site radii $R_B = 0.3$–1.1 Å, depending upon the relative sizes of R_A and R_B. Usually there is little exchange between the A- and B-type atoms but in certain situations when A_n and B_n are similar in size and/or there is extensive oxygen disorder, A/B antisite disorder can occur. There are many examples in the literature. Two applicable examples of this are (1) LeComte, Loup, Hervieu, and Raveau[42] found that Sr occupied both A and B sites in Sr $(Sr_{1/3+x}Nb_{2/3-x})O_{3-y}$ and was sensitive to temperature and oxygen partial pressure and (2) Battle[43] used neutron diffraction to show that in $Ca(La_{1/2}Ru_{1/2})O_3$ the A sites were occupied by Ca and La in a disordered manner and the B sites were occupied by an ordered array of Ca and Ru. The respective atomic radii and neutron scattering lengths are shown in Table IV for these elements and for those in La-Sr-Cu-O and Y-Ba-Cu-O. From consideration of Table IV and the examples it is clear that elements can have a range of effective sizes depending on their coordination geometry. Also, when the scattering lengths are sufficiently different, i.e., 50% as for Ca and Ru, neutron diffraction has detected antisite disorder in a compound which has ions very similar in size to the high-T_c $YBa_2Cu_3O_7$. In the other example, Sr $(Sr_{1/3-x}Nb_{2/3-x})O_3$, when extensive oxygen disorder was present Sr could occupy the B site even though it is a large atom. Of course La-Sr-Cu-O and Y-Ba-Cu-O are not perovskites but do share essential similarities. For illustration of antisite disorder these two examples are fair structural analogues of the superconducting compounds. To emphasize the point, antisite disorder in perovskites is not unusual, it was just not considered in determining the structure of La-Sr-Cu-O and Y-Ba-Cu-O.

The usual techniques for structure determination, x-ray and neutron diffraction, have well-known strengths and important weaknesses. When the sample is illuminated by the beam all of the atoms scatter a part of it, depending upon the scattering strength of each atom. For elements that scatter about the same, it is impossible to tell them apart. This is the case for neutron diffraction for the high-T_c structures which have been determined thus far. The neutron scattering lengths are given in Table IV. Obviously, Cu and Y are indistinguishable. In the compounds $La_{1.8}(Sr_{0.2}$ or $Ba_{0.2})CuO_4$ the weighted averages of the scattering lengths for $La_{1.8}+Sr_{0.2}$ or $La_{1.8}+Ba_{0.2}$ are 0.81 and 0.80, respectively. If the substitution of Sr or Ba into the La site is random, then the scattering from those atoms is only 5% different than if Cu was in that site, which is not much contrast. Obviously, to detect disorder (or order) with neutron diffraction a compound must be chosen with sufficient diffraction contrast, e.g., with Yb or Gd.

TABLE IV. Selected atomic radii (Ref. 56) and neutron scattering lengths (Ref. 57).

Element	Coordination no.	Radius (Å)	Scattering length (10^{-12} cm)
O^{2-}	6	1.40	0.58
Cu^{2+}	4 (square planar)	0.62	0.76
	6	0.73	
Y^{3+}	6	0.89	0.79
	8	1.02	
La^{3+}	6	1.06	0.83
	12	1.32	
Nb^{4+}	6	0.69	0.71
Ru^{4+}	6	0.62	0.73
Ca^{2+}	6	1.00	0.49
	12	1.35	
Sr^{2+}	6	1.16	0.69
	12	1.44	
Ba^{2+}	6	1.36	0.52
	12	1.60	

The scattering factor for x rays is different for each of these atoms and x-ray diffraction, in principle, should locate them. The problems here are the limitations of the Rietveld refinement technique[44] for powder data. Particular difficulties are the unknown diffracted peak profile[45] and the impossibility of separating thermal scattering from the background. This requires that the profile and background parameters be a part of the fit to the data. Most important, however, is the bias of the solution toward the trial structure. Unless antisite disorder is suspected and tried it will not be detected. This is true for any x-ray or neutron-diffraction technique, although good, single-crystal x-ray data should detect the disorder effect. Specifically, there are conflicting reports of the structure of La_2CuO_4 in the literature,[46–48] all from powder data. The recent structure determination of La-Sr-Cu-O (Ref. 32) and $La_{1.85}Ba_{0.15}CuO_4$ (Ref. 49) used neutron-diffraction powder data which are insensitive to disorder. However, note that the Cu or La exchange in the series of $La_{2-x}Sr_xCuO_4$ compounds by Nguyen, Choisnet, Hervieu, and Raveau[50] would explain the anomalous increase in the c axis with increasing Sr (Fig. 3, Ref. 50). The x-ray single-crystal determination of Y-Ba-Cu-O (Ref. 33) was on a small crystal with 418 reflections measured. If the crystal was truly untwinned, this data should be adequate to show the Cu/Y substitution effect.

In contrast to these diffraction methods x-ray-absorption spectroscopy is atomic species specific. The x-ray energy can be tuned to each element in turn and its structure determined either from the XANES or EXAFS. However, as was shown these techniques are sensitive only to the short-range structure around the absorbing atom. The best that can be done is a radial distribution function centered on the absorbing atom and averaged over the different atomic sites (when more than one) of that atom.

For La-Sr-Cu-O and Y-Ba-Cu-O this was sufficient to identify a unique Cu distance with a particular lattice site.

DISCUSSION

A model for interpreting the XANES was developed from data for reference compounds of simple structure chosen to both maximize and minimize the occurrence of MS. This allowed identification of XANES features with specific bond distances. The model is nothing more than identifying the XANES (excluding bound-state structure) as the first EXAFS bump superimposed upon the smooth rise of the continuum. The first EXAFS cycle has a certain uniqueness in that the electron wavelength is equal to the bond distance for the first n coordination shells without the complication of superimposed higher orders of scattering. This is also the energy where the cross section for scattering is highest. It is not the whole story, multiple scattering is also present to a lesser degree, but is a useful approximation in that bond distances may be read by inspection without recourse to Fourier transforms. Also, for bonds with large thermal disorder the first bump may contain most of the detectable scattering. Thus, the structure up to $\lambda = R_{\min}$ above threshold is an image $E \propto 1/R^2$ of the lattice surrounding the absorbing atom superimposed upon the underlying, smooth arctangent of the continuum. The energy position of the scattering resonances on top of the arctangent is pure coincidence due only to the match between the electron wavelength and the bond distances of the specific lattice environment. XANES features from other compounds with longer or shorter bonds or with a different position for $E = 0$ will move the resonance peaks back and forth, appropriately, on top of the edge. The apparent close agreement with the $\lambda = R$ condition is somewhat surprising; however, the deviation from the $\lambda = R$ curve represents what is usually called the phase shift and shows similar trends with atomic number and valence as the higher energy EXAFS phase shifts. We expect that similar E vs R or $1/R^2$ correlations will apply for absorption edges at much lower or higher energies.

The distinguishing 7 eV doublet at the top of the La-Sr-Cu-O and Y-Ba-Cu-O absorption edges had been attributed to overlap of the Cu^{+2} and Cu^{+3} absorption edges.[4] Our new understanding of XANES allowed us to recognize that the higher energy bump at ~ 25 eV was due to a scattering resonance from an unexpected Cu–O distance of ~ 2.6 Å. This distance places a significant fraction of the Cu in the Y or La site as the case may be and totally changes our concept of these materials and how they conduct. Cu ions in the La and Y sites suggest a number of possibilities. The small Cu radius relative to Y or La give Cu easy access to the site where it could vibrate freely responding to local forces, i.e., a soft mode. The disorder associated with this distance should be sensitive to temperature. When Cu occupies the Y or La site in either structure a body-centered Cu atom sublattice is completed (reminiscent of the $A15$ structure) with the distance of nearest approach for Cu-Cu along the body diagonal of 3.25 Å in La-Sr-Cu-O (Ref. 32) and 3.20 Å in Y-Ba-Cu-O.[33] Our work in progress shows this to be a very soft mode.[37] Note that there are no directly intervening oxygen atoms. In Y-Ba-Cu-O the missing oxygen from the Cu_2 octahedra opens up the lattice between Cu_2 and the Y site. This is shown in Fig. 11. Conversely, with the Cu on the Y or La sites Y or La must occupy the Cu sites. The discussion of size tolerances in perovskitelike materials given previously indicates that this is plausible given the range in sizes of the ions considered. Therefore, the smaller M^{3+} ions will exchange into the Cu sites easily and only with difficulty when they are much larger. This may explain the small effect on T_c of the equisized

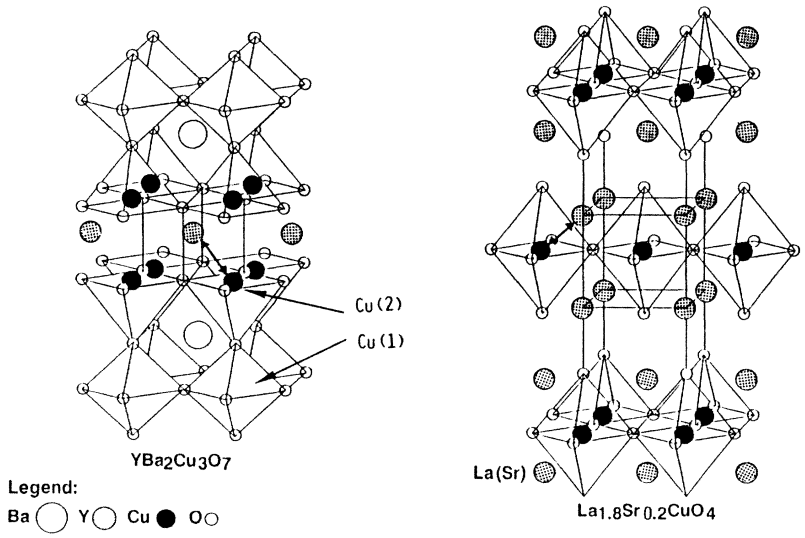

FIG. 11. Perspective drawings based upon crystal structure determinations for Y-Ba-Cu-O (Ref. 33) and La-Sr-Cu-O (Ref. 32). In each the actual size of the oxygen atoms has been reduced in order to view the metal atom lattice. Compare with Table III. The antisite exchange is indicated.

rare-earth ions.[51,52] It follows that solid-state preparation is rate limited by diffusion of M^{3+} into the octahedral hole and that the total amount of exchange must balance the ionic sizes and the stability of the structure. Our inspection of the published Cu K-edge data[3,4] of La_2CuO_4 shows that Cu is also in the La site in this compound. Also, the anomalous c-axis expansion in the $La_{2-x}Sr_xCuO_4$ series was found to be a maximum when $X=\frac{1}{3}$ (Ref. 50) which suggests that $\frac{1}{3}$ mole fraction is the maximum substitution of La into the Cu site and vice versa. It remains to be proved whether the observed antisite disorder in these compounds is related to or essential for their observed superconductivity. Our projection is that it will be. The probability of a soft phonon mode directly linking the Cu atoms must be significant. In these compounds there may be two criteria for superconductivity: (1) Cu in the La or Y site which connects the Cu layers and (2) simultaneous Cu^{2+} and Cu^{3+}.[53-55]

ACKNOWLEDGMENTS

We thank Stanford Synchroton Radiation Laboratory, which is funded by Department of Energy, for beam time. The research of F.W.L. was funded by National Science Foundation Grant No. CHE8219605 and that of R.B.G. by Department of Energy Grant No. DE-FG06-84ER45121.

[1]U. C. Srivastava and H. L. Nigam, Coord. Chem. Rev. **9**, 275 (1973).
[2]H. Oyanagi, H. Ihara, T. Matsushita, M. Tokumoto, M. Hirabayashi, N. Terada, K. Senzaki, Y. Kimura, and T. Yao, Jpn. J. Appl. Phys. **26**, L488 (1987).
[3]J. M. Tranquada, S. M. Heald, A. Moodenbaugh, and M. Suenaga, Phys. Rev. B **35**, 7187 (1987).
[4]E. E. Alp, G. K. Shenoy, D. G. Hinks, D. W. Capone II, L. Soderholm, H. B. Schattler, J. Guo, D. E. Ellis, P. A. Montano, and M. Ramanathan, Phys. Rev. B **35**, 7199 (1987).
[5]H. Oyanagi, H. Ihara, T. Matsushita, M. Tokumoto, M. Hirabayashi, N. Terada, K. Senzaki, Y. Kimura, and T. Yao, Jpn. J. Appl. Phys. **26**, L638 (1987).
[6]A. J. Panson, G. R. Wagner, A. I. Braginski, J. R. Gavaler, M. A. Janocko, H. C. Pohl, and J. Talvacchio, Appl. Phys. Lett. **50**, 16 (1987).
[7]A. J. Panson, A. I. Braginski, J. R. Gavaler, J. K. Hulm, M. A. Janocko, H. C. Pohl, A. M. Stewart, J. Tavacchio, and G. R. Wagner, Phys. Rev. B **35**, 8774 (1987).
[8]A. I. Braginski, in *Novel Superconductivity*, Proceedings of the International Workshop on Novel Mechanisms of Superconductivity, Berkeley, 1987, edited by S. A. Wolf and V. Z. Kresin (Plenum, New York, 1987), p. 935.
[9]A. J. Panson (unpublished), but summarized in Ref. 8.
[10]A. Manthiram, J. S. Swinnea, Z. T. Sui, H. Steinfink, and J. B. Goodenough (unpublished).
[11]F. Sette, J. Stöhr, and A. P. Hitchcock, Chem. Phys. Lett. **110**, 517 (1984).
[12]J. Stöhr, F. Sette, and A. L. Johnson, Phys. Rev. Lett. **53**, 1684 (1984).
[13]A. Bianconi, E. Fritsch, G. Calas, and J. Petiau, Phys. Rev. B **32**, 4292 (1985).
[14]R. B. Greegor, F. W. Lytle, D. R. Sandstrom, J. Wong, and P. Schultz, J. Non-Cryst. Solids **55**, 27 (1983).
[15]C. R. Kurkjian, J. Non-Cryst. Solids **3**, 157 (1970).
[16]R. M. Friedman, J. J. Freeman, and F. W. Lytle, J. Catal. **55**, 10 (1978).
[17]R. W. G. Wyckoff, *Crystal Structures*, 2nd ed. (Interscience, New York, 1963).
[18]J. E. Hahn, R. A. Scott, K. O. Hodgson, S. Doniach, S. Desjardins, and E. I. Solomon, Chem. Phys. Lett. **88**, 595 (1982).
[19]F. W. Kutzler, R. A. Scott, J. M. Berg, K. O. Hodgson, S. Doniach, S. P. Cramer, and C. H. Chang, J. Am. Chem. Soc. **103**, 6083 (1981).
[20]G. A. Waychunas, Am. Mineral. **72**, 89 (1987).
[21]J. Wong, F. W. Lytle, R. P. Messmer, and D. H. Maylotte, Phys. Rev. B **30**, 5596 (1984).
[22]L. S. Kau, D. J. Spira-Solomon, J. E. Penner-Hahn, K. O. Hodgson, and E. I. Solomon, J. Am. Chem. Soc. **109**, 6433 (1987).
[23]A. Bianconi, M. Dell'Ariccia, A. Gargano, and C. R. Natoli, in *EXAFS and Near-Edge Structure*, edited by A. Bianconi, L. Incoccia, and S. Stipcich, Springer Series in Chemical Physics, Vol. 27 (Springer, Berlin, 1983), p. 57.
[24]D. Norman, J. Stöhr, R. Jaeger, P. J. Durham, and J. B. Pendry, Phys. Rev. Lett. **51**, 2052 (1983).
[25]J. E. Muller and W. L. Schaich, Phys. Rev. B **27**, 6489 (1983).
[26]J. Stöhr, J. L. Gland, W. Eberhardt, D. Outka, R. J. Madox, F. Sette, R. J. Koestner, and U. Doebler, Phys. Rev. Lett. **51**, 2414 (1983).
[27]G. Bunker and E. A. Stern, Phys. Rev. Lett. **52**, 1990 (1984).
[28]J. J. Boland, S. E. Crane, and J. D. Baldeschweiler, J. Chem. Phys. **77**, 142 (1982).
[29]I. Lindau and W. E. Spicer, J. Electron Spectrosc. Relat. Phenom. **3**, 409 (1974).
[30]V. W. Hu, S. I. Chan, and G. S. Brown, Proc. Natl. Acad. Sci. **74**, 3821 (1977).
[31]R. B. Greegor, F. W. Lytle, A. J. Panson, and J. Stöhr (unpublished).
[32]R. J. Cava, A. Santoro, D. W. Johnson, Jr., and W. W. Rhodes, Phys. Rev. B **35**, 6716 (1987).
[33]Y. LePage, W. R. Mckinnon, J. M. Tarascon, L. H. Greene, G. W. Hull, and D. M. Hwang, Phys. Rev. B **35**, 7245 (1987).
[34]P. A. Lee, P. H. Citrin, P. Eisenberger, and B. M. Kincaid, Rev. Mod. Phys. **53**, 769 (1981).
[35]G. Beni and P. Platzmnn, Phys. Rev. B **14**, 1514 (1976).
[36]S. Asbrink and L. J. Norrby, Acta Crystallogr. B **26**, 8 (1970).
[37]F. W. Lytle, R. B. Greegor, and A. Mansour (unpublished).
[38]J. B. Boyce, F. Bridges, T. Claeson, T. H. Geballe, C. W. Chu, and J. M. Tarascon, Phys. Rev. B **35**, 7203 (1987).
[39]J. M. Tranquada, S. M. Heald, and A. R. Moodenbaugh, Phys. Rev. B (to be published).
[40]J. A. Yarmoff, D. R. Clarke, W. Drube, U. O. Karlsson, A. Taleb-Ibrahimi, and F. J. Himpsel, Phys. Rev. B **36**, 3967 (1987).
[41]F. W. Lytle, R. B. Greegor, and A. J. Panson, in Ref. 8, p. 1049

[42]J. LeComte, J. P. Loup, M. Hervieu, and B. Raveau, Phys. Status Solidi **65**, 743 (1981).
[43]P. D. Battle, Mater. Res. Bull. **16**, 397 (1981).
[44]A. Albinati and B. Willis, J. Appl. Crystallogr. **15**, 361 (1982).
[45]R. A. Young and D. B. Wiles, J. Appl. Crystallogr. **15**, 430 (1982).
[46]V. B. Grande, H. K. Muller-Buschbaum, and M. Schweizer, Z. Anorg. Allg. Chem. **428**, 120 (1977).
[47]K. K. Singh, P. Ganguly, and J. B. Goodenough, J. Solid State Chem. **52**, 254 (1984).
[48]J. M. Longo and P. M. Raccah, J. Solid State Chem. **6**, 529 (1973).
[49]J. O. Jorgenson, H. B. Schuttler, D. G. Hinks, D. W. Capone II, K. Ihang, and M. B. Brodsky, Phys. Rev. Lett. **58**, 1024 (1987).
[50]N. Nguyen, J. Choisnet, M. Hervieu, and B. Raveau, J. Solid State Chem. **39**, 120 (1981).
[51]R. H. Hor, R. L. Meng, Y. O. Wang, L. Gao, Z. J. Huang, J. Bechtold, K. Forster, and C. W. Chu, Phys. Rev. Lett. **58**, 1891 (1987).
[52]D. W. Murphy, S. Sunshine, R. B. vanDover, R. J. Cava, B. Batlogg, S. M. Zahurak, and L. F. Schneemeyer, Phys. Rev. Lett. **58**, 1888 (1987).
[53]J. G. Bednorz and K. A. Müller, Z. Phys. B **64**, 189 (1986).
[54]P. W. Anderson, Science **235**, 1196 (1987).
[55]L. Pauling, Phys. Rev. Lett. **59**, 225 (1987).
[56]R. D. Shannon and C. P. Prewitt, Acta Crystallogr. **25**, 925 (1969).
[57]*International Tables for X-ray Crystallography* (Kynoch, Birmingham, England, 1974), Vol. 4, p. 270.

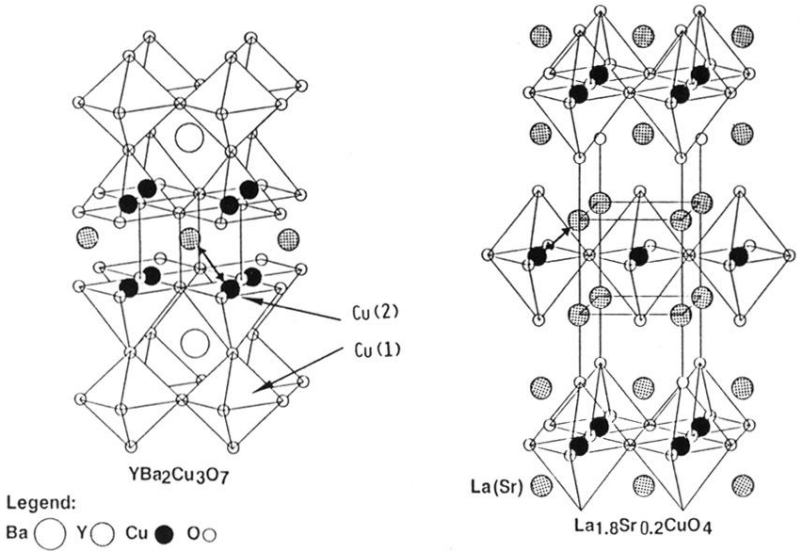

FIG. 11. Perspective drawings based upon crystal structure determinations for Y-Ba-Cu-O (Ref. 33) and La-Sr-Cu-O (Ref. 32). In each the actual size of the oxygen atoms has been reduced in order to view the metal atom lattice. Compare with Table III. The antisite exchange is indicated.